**HADRONIC FINAL STATES IN PHOTOPRODUCTION AND THE STRUCTURE OF THE REAL AND VIRTUAL PHOTON**

**Wieland Hoprich**
*Max-Planck-Institut für Kernphysik*
*Saupfercheckweg 1*
*69117 Heidelberg, Germany*

**(representing the H1 Collaboration)**

Measurements of the structure of quasi real and virtual photons with the H1 detector at HERA are presented. The double differential dijet cross section in quasi real photoproduction is determined and an effective leading order parton density is extracted. The mesurement of inclusive charged particle spectra in photoproduction and a new method to extract the gluon density of the photon based on this measurement are presented. The triple differential dijet cross section is measured in deep inelstic scattering processes and an effective leading order parton density of the virtual photon is extracted as a function of the photon virtuality, the probing scale and the parton momentum fraction.

# 1 Introduction

The positron-proton collider HERA offers a unique possibility to study the hadronic structure of the photon. Measurements of the photon structure function $F_2^\gamma$ in $e^+e^-$ interactions are sensitive to its quark densities. When the partons of the proton are used as the probe the measurement is sensitive to both the quark and gluon densities of the photon. Hadronic final states in hard processes such as dijet events or events with high $p_T$ tracks have been shown to be sensitive to the hadronic structure of the photon. They are used to investigate its parton densities.

# 2 Dijets Cross Section and Effective Parton Distrubution of the Quasi Real Photon

The double differential dijet cross section in real photoproduction ($Q^2 < 4\,\mathrm{GeV}^2$) has been measured by H1. Jets were found by a cone algorithm [1] with cone size $R = 0.7$ and jet pseudo rapidities in the range $-0.5 < \eta < 2.5$. The average transverse jet energy $E_T^{jets}$ had to be larger than 10 GeV. Photon fractional energies were restricted to the range $0.2 < y < 0.83$.

The result of the measurement is shown in Fig.1 as a function of $E_T^{jets}$ in different bins of the reconstructed parton fractional energy $x_\gamma^{jets} = \sum_{jets} E_T^{jet} e^{-\eta^{jet}}/2E_\gamma$.

The data are compared to a leading order simulation of the PYTHIA [2] generator using the GRV-LO parton distribution functions and to analytical next-to-leading order (NLO) calculations using the GRV-HO and GS96 parton distributions of the photon. The theoretical predictions give a satisfactory description of the data except for the two highest bins in $x_\gamma^{jets}$. In this region the resolved photon contribution is not well constrained from measurements of the photon structure function $F_2^\gamma$ in $e^+e^-$ collisions. The data presented in Fig.1 give new constraints on the parton distribution functions in the region at large $x_\gamma^{jets}$ and high $E_T^{jets}$.

Parton distributions of the photon were extracted using an approximation method developed in [3]. The shapes of the angular distribution of the scattered partons are similar for all the leading order matrix elements for the partonic scattering processes $qq' \to qq'$,$qg \to qg$ and $gg \to gg$ giving the dominant contribution to the total resolved photon dijet cross section. The approximation uses only one Single Effective Subprocess matrix element $M_{\mathrm{SES}}$ and combines the quark and gluon densities into new effective parton density functions $\tilde{f}_\gamma$ and $\tilde{f}_p$.

$$\tilde{f}(x, p_T^2) = \sum_{n_f} \left( q(x, p_T^2) + \bar{q}(x, p_T^2) \right) + \frac{9}{4} g(x, p_T^2)$$

Here, $p_T$ is the transverse momentum of the final state partons; it is taken to be the scale of the process. The distribution $\tilde{f}(x, p_T^2)$ can be directly determined from the measurement of the di-parton cross section.

The leading order effective parton distribution of the photon is shown in Fig.1. The data show the logarithmic increase of the photon structure on the scale $p_T^2$ as expected from the anomalous photon contribution [4]. The GRV-LO parametrisation of the photon (full line) reproduces the measurement. The dotted line shows the contribution from quarks only in the resolved photon. Since the quark density in the shown region of $x_\gamma$ is well constrained by $e^+e^-$ experiments the difference between this and the measured values is a consequence of the gluon content of the photon. It contributes about 20% to the total effective parton density distribution in the range $0.4 < x_\gamma < 0.7$ and about 50% in the range $0.2 < x_\gamma < 0.4$.

## 3 Charged Particle Cross Section and the Gluon Density in the Quasi Real Photon

Inclusive charged particle production has been studied by H1. For this analysis the scattered positron was required to be detected in the fiducial volume of the electron tagger of the H1 luminosity system. Consequently those events have a four-momentum transfer $Q^2 < 10^{-2}\,\mathrm{GeV}^2$. The events were required to have $0.3 < y < 0.7$. Tracks were selected which have a transverse momentum with respect to the beam axis of at least $2\,\mathrm{GeV/c}$ and a pseudorapidity measured in the HERA laboratory reference system of $|\eta| < 1$.

The dependence of this cross section on the transverse momentum is shown in Fig.2.

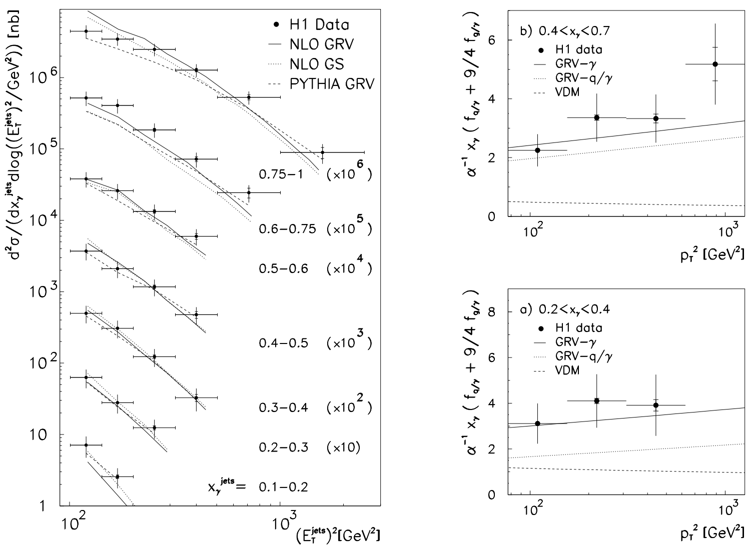

Fig. 1: **Left:** The dijet cross section as a function of the average transverse jet energy squared in different bins of $x_\gamma$ compared to a LO QCD simulation and to analytical next-to-leading order calculations. **Right:** The LO effective parton distribution of the photon as a function of the parton transverse momentum $p_T^2$ in two different ranges of $x_\gamma$. The data are compared to the effective parton distribution calculated using the GRV parton distribution function of the photon (full curve) and its quark contribution (dotted curve). The dashed curve shows a pure VMD ansatz for the photon.

The QCD inspired power-law expression

$$\frac{d^2\sigma_{\gamma p}}{dp_T^2 d\eta} = A(1 + \frac{p_T}{(p_T)_0})^{-n}$$

was fitted to the data giving a good description over the whole $p_T$ range. Also shown are the results of similar fits to $p\bar{p}$ collider data at CMS energies between $\sqrt{s} = 200\,\mathrm{GeV}$ and $\sqrt{s} = 1800\,\mathrm{GeV}$. The hardness of the $\gamma p$ spectrum is comparable to that in $p\bar{p}$ collisions at the highest energy and is clearly larger than that in $p\bar{p}$ collisions at similar CMS energy. This behaviour can be understood as being due to extra contributions in $\gamma p$, namely the direct and anomalous resolved component.

In Fig.2 the ratio of the data to an analytical NLO calculation [5] using the GRV parametrisation of the parton density function of the photon [6] and proton [7] is shown. Renormalisation and factorisation scales were chosen to be $p_T^2$. The effect of this choice is shown by predictions for a scale of $\xi p_T^2$ with $\xi = 0.5$ and 2, shown as a ratio to the prediction for $\xi = 1$.

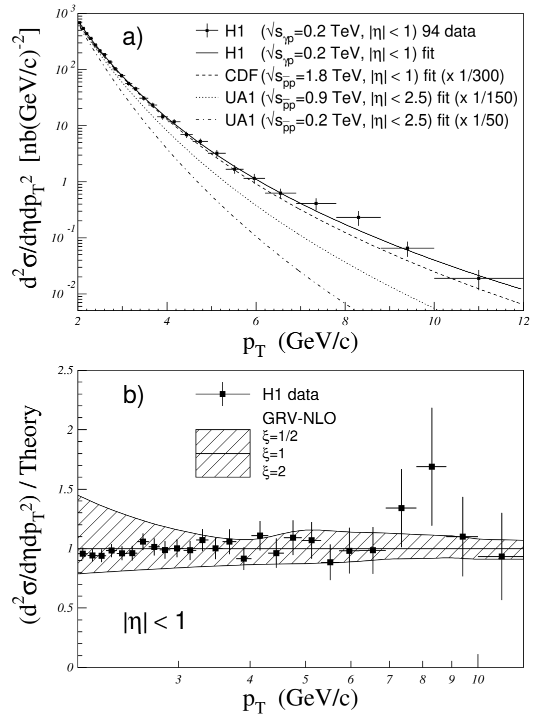


Fig. 2: **a)** The inclusive $\gamma p$ cross section for charged particles in photoproduction. The curves indicate power-law fits for these data and for $p\bar{p}$ data (see text). **b)** The ratio of data over the NLO QCD calculation with scale $\xi p_T^2$ for $\xi = 1$. The shaded band shows the expected variation of the ratio as $\xi$ changes from 0.5 to 2.

The dependence of the cross section on the pseudo rapidity is shown in Fig.3 for $p_T > 2\,\mathrm{GeV/c}$ and $p_T > 3\,\mathrm{GeV/c}$. The data are compared with predictions of LO QCD calculations made with PYTHIA [2] for different structure functions of the photon and assumptions on the soft interactions in the underlying event. All structure functions except LAC1 [8] show a falling distribution with increasing $\eta$ contrary to data. For $p_T > 2\,\mathrm{GeV}$ there is a strong sensitivity to the parton distribution of the photon and also to the amount of underlying interactions. None of the predictions presented shows satisfactory agreement with the data. For $p_T > 3\,\mathrm{GeV}$ data agree best with LAC1. The sensitivity to the photon structure is reduced but still significant and the effect of multiple interaction becomes very small.

The distribution of the momentum fraction $x_\gamma = E_{parton}/E_\gamma$ of the parton of the photon entering the hard subprocess was determined from the inclusive charged particle data. Events were kept which have at least one track with $p_T > 2.6\,\mathrm{GeV/c}$. For each

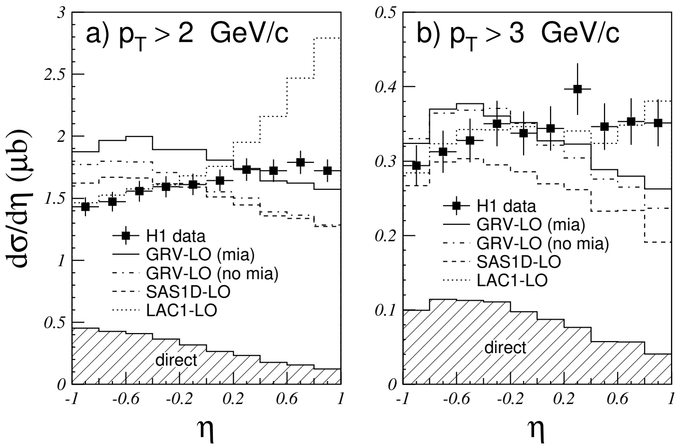


Fig. 3: The differential $\gamma p$ cross section $d\sigma/d\eta$ for inclusive production of high $p_T$ charged particles compared to LO QCD predictions of PYTHIA using different parton density distributions. The contributions from the direct photon processes are shown as shaded histograms.

of those events the variable

$$x_\gamma^{rec} = \frac{\sum p_T e^{-\eta}}{E_\gamma}$$

was calculated where the sum runs over all tracks with $p_T > 2\,\mathrm{GeV/c}$. This variable is correlated to the true $x_\gamma$ of the interaction. For the reconstruction of the true $x_\gamma$ an unfolding procedure [9] was used. In Fig.4 the result is shown in three bins of $x_\gamma$ with statistical errors only which include the bin-to-bin correlations. The dotted curve is the prediction of PYTHIA with the LAC1 parton distribution of the photon while the dashed curve represents the event rate where only quarks from the photon side are involved. The quark distribution in the photon is rather well constrained from $e\gamma$ measurements as discussed in Section 2. With the assumption of data and prediction differing due to the theoretical uncertainty in the gluon density the gluon density in the photon was extracted. The result is shown in Fig.5. The average transverse momentum squared of the of the hard partonic scattering was taken as the scale. As derived from Monte Carlo studies it amounts to $< p_T^2 >= 38\,\mathrm{GeV^2/c^2}$. The result is compared with various parton distributions and with a measurement based on the 1993 H1 data using dijet events. The measurements are in good agreement but the measurement using tracks shows a significantly higher precision. It avoids two large systematic errors entering the jet analysis which are the uncertainty of the energy scale of the calorimeter and the uncertainty due to overlap with energy depositions from soft multiple interactions. The drawback of this method is a stronger sensitivity to fragmentation uncertainties.

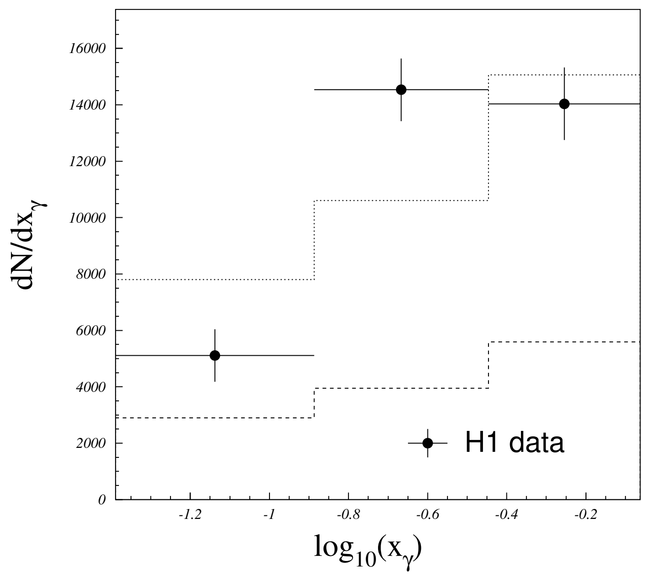


Fig. 4: The $x_\gamma$ distribution of the photon. The curves are full (dotted line) and "quark only" predictions of PYTHIA, using the LAC1 parton distribution of the photon.

# 4 Dijet Cross Section and Effective Parton Distribution of the Virtual Photon

In deep inelastic scattering (DIS) when the exchanged photon is highly virtual its interaction is usually interpreted as that of a pointlike object. However, if the photon is probed with sufficiently high resolution, i.e. if jets are produced with $P_t^2 \gg Q^2$, it is still possible to have interactions in which its structure is resolved. It is a prediction of perturbative QCD that the parton densities of virtual photons become suppressed with increasing $Q^2$.

In the analysis presented simulated events produced by HERWIG [10] and RAPGAP [11] were used to correct the measured cross section for detector effects and to compare the data with the predictions of various theoretical models. The factorisation scales of the proton and photon parton densities were set to the $P_t$ of the scattered partons. GRV parton densities were used for the proton. Several models for the virtual photon parton densities were considered.

The Drees-Godbole model [12] starts with parton densities of the real photon and suppresses them by a factor $\mathcal{L}$ defined as:

$$\mathcal{L}(Q^2, P_t^2, \omega) = \frac{\ln((P_t^2 + \omega^2)/(Q^2 + \omega^2))}{\ln((P_t^2 + \omega^2)/\omega^2)}$$

Quark densities in the real photon are suppressed by $\mathcal{L}$ and the gluon density by $\mathcal{L}^2$.

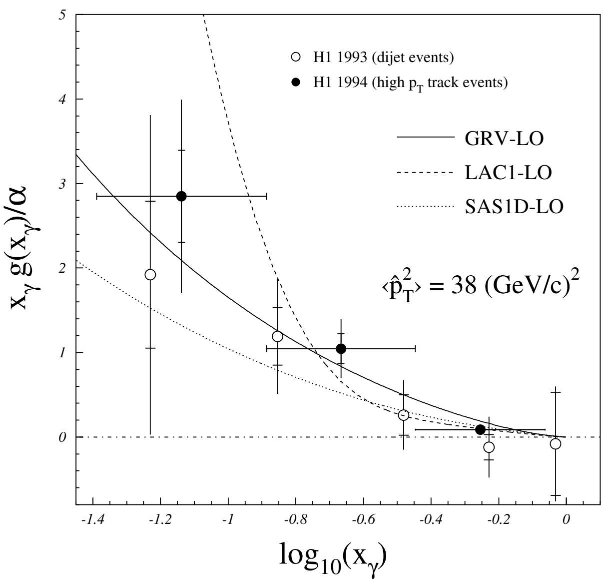


Fig. 5: Two measurements of the LO gluon density in the photon using high $p_T$ charged particles (full circles) and dijet events (open circles). The full line shows the parametrisation of GRV, the dotted line SAS1D and the dashed line LAC1.

This ansatz is designed to make a smooth interpolation between the leading logarithmic part of the real photon parton densities $\sim \ln(P_t^2/\Lambda_{QCD}^2)$ and the asymptotic domain, $P_t^2 \gg Q^2 \gg \Lambda_{QCD}^2$, where the parton densities are predicted to behave as $\sim \ln(P_t^2/Q^2)$. It was found in this analysis that values $\sim 0.1 - 0.2\,\mathrm{GeV}$ for the free parameter $\omega$ give a reasonable description of the data.

In the model of Schuler and Söstrand [13] the parton densities of the virtual photon are decomposed into a non-perturbative and a perturbative part. The non-perturbative part is modelled by vector-meson-dominance (VMD) and is rapidly suppressed by a factor $\sim (m_V^2/(m_V^2+Q^2))^2$, whereas the perturbative part has a logarithmic suppression designed to approach the exact QCD prediction in the region where $P_t^2 \gg Q^2 \gg \Lambda_{QCD}^2$.

The dijet cross section in the range $1.6 < Q^2 < 80\,\mathrm{GeV}^2$ has been measured by H1. In this analysis events were required to have $0.1 < y < 0.7$. Jets were found using the inclusive $k_t$-algorithm [14] in the $\gamma^* p$ frame. Events were accepted if the two highest $E_t$ jets in the event satisfied the following kriteria:$|\eta^{jet1} - \eta^{jet2}| < 1.0$; $-3.0 < \bar{\eta} < -0.5$; $\bar{E}_t^2 > 30\,\mathrm{GeV}^2$; $|(E_t^{jet1} - E_t^{jet2})|/(E_t^{jet1} + E_t^{jet2}) < 0.25$. $E_t$ and $\eta$ are always given with reference to the $\gamma^* p$ CMS. The dijet cross section was measured in dependence of the variables $x_\gamma$, $\bar{E}_T^2$ and $Q^2$. It was corrected for detector effects by applying a Bayesian two-dimensional unfolding technique [15].

The triple differential cross section is shown in Fig.6 as a function of $x_\gamma^{jets}$ and in Fig.7 as a function of $Q^2$, in each case in bins of the other two variables. In Fig.6

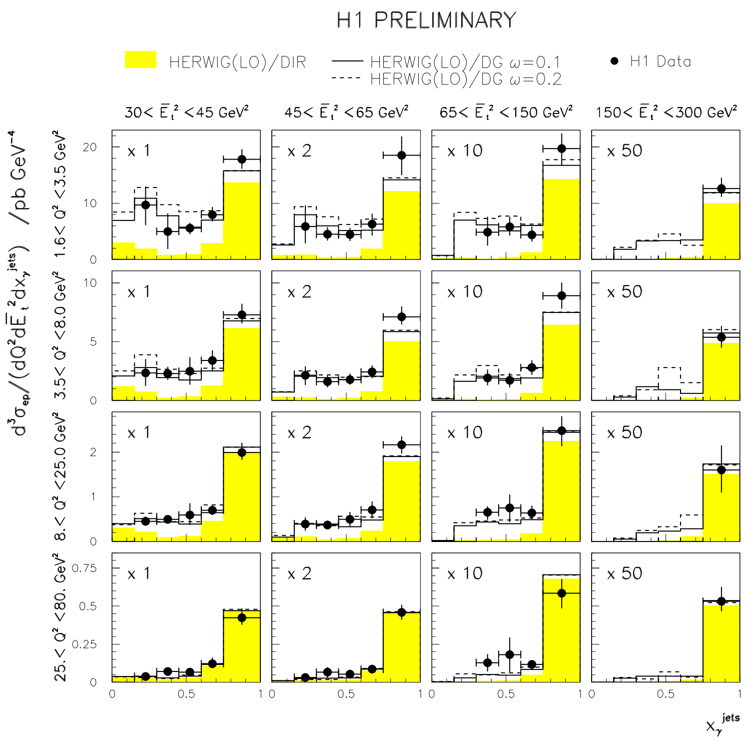


Fig. 6: The differential dijet cross section as a function of $x_\gamma^{jets}$ for different regions of $\bar{E}_t^2$ and $Q^2$. Also shown is the HERWIG(LO)/DG model with two choices of $\omega$ and 10% soft underlying event.

the $x_\gamma^{jets}$ distributions peak towards $x_\gamma^{jets} = 1$. There is a strong decrease of the cross section with increasing $\bar{E}_t^2$. The relative contribution from resolved photons in the region $x_\gamma^{jets} < 0.75$ diminishes as $Q^2$ increases at fixed $\bar{E}_t^2$. The data are well reproduced by the HERWIG(LO)/(DG) model with $\omega \sim 0.1 - 0.2$. In Fig.7 the steep decrease of the cross section with $Q^2$ is shown. The rate of decrease becomes smaller as $x_\gamma^{jets}$ increases and is well reproduced by the RAPGAP(LO)/DG model.

In a second step the Bayesian unfolding method was applied again to extract the effective parton densities of the virtual photon, correcting the dijet cross section to the leading order diparton cross section. It uses correlations between $\{x_\gamma^{jets}, \bar{E}_T\}$ and $\{x_\gamma, P_t\}$.

The extracted effective parton density is shown in Fig.8 as a function of $Q^2$ for $P_t^2 = 85\,\mathrm{GeV}^2$, in the upper figure for $0.35 < x_\gamma < 0.5$ and in the lower for $0.5 < x_\gamma < 0.7$. Superimposed on the same plots are photoproduction data obtained from the analysis presented in Section 2 which have been extrapolated to the $P_t^2$ and $x_\gamma$ values in the figures. The evolution with $Q^2$ is compared with that predicted by the models

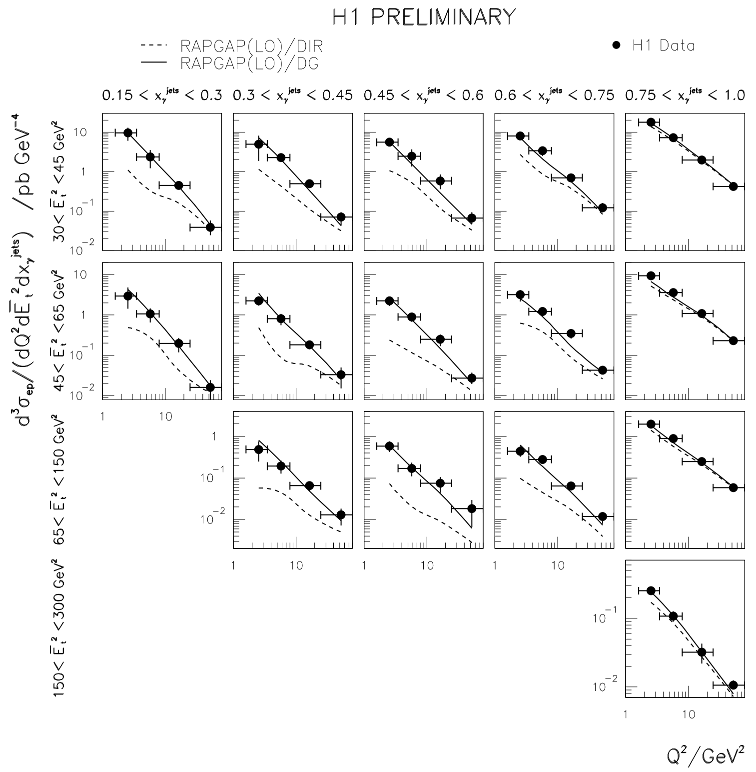


Fig. 7: The differential dijet cross section as a function of $Q^2$ for different regions of $x_\gamma^{jets} and \bar{E}_t^2$. Also shown is the RAPGAP(LO)/DG model (full curve). The dashed curve shows the prediction for the direct photon process.

mentioned above and with a simple $\rho$-pole suppression factor characteristic of a pure VMD model:

$$f_{i|\gamma}(x_\gamma, P_t^2, Q^2) \sim f_{i|\gamma}(x_\gamma, P_t^2, 0) \left( \frac{m_\rho^2}{m_\rho^2 + Q^2} \right)^2 .$$

The latter clearly underestimates the data. Within the experimental errors the parametrisations of the parton distributions of virtual photons describe the measured data.

## References


[1] J. Huth et al.: *Fermilab-Conf-90/249-E* (1990) ;

[2] T. Sjöstrand: *Comput. Phys. Commun.* **82** (1994) 74;

[3] B.L. Combridge, C.J. Maxwell: *Nucl. Phys.* **B 239** (1984) 429;

[4] E. Witten: *Nucl. Phys.* **B120** (1977) 189;

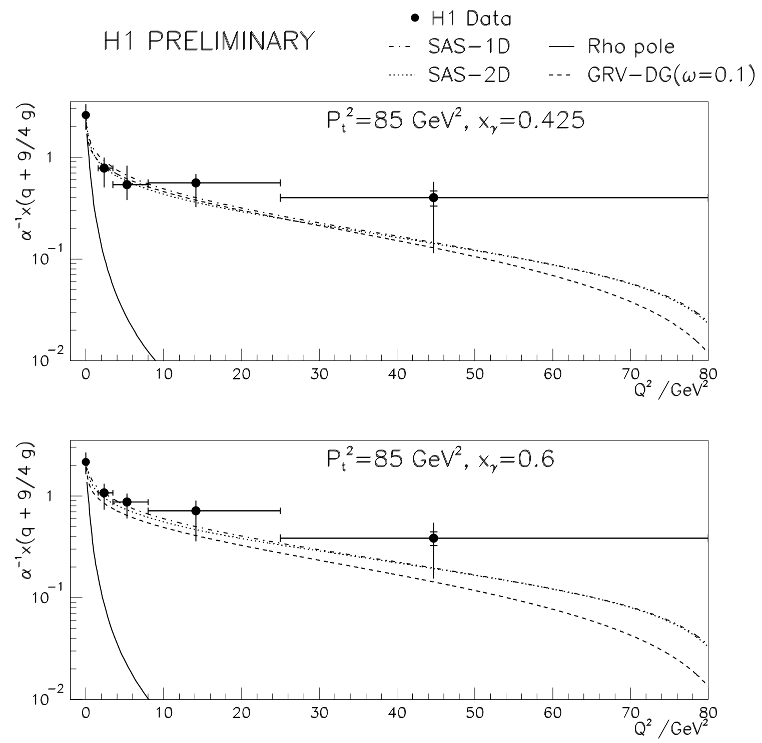


Fig. 8: The leading order effective parton density of the photon as a function of $Q^2$ for $P_t^2 = 85\,\mathrm{GeV}^2$ and two values of $x_\gamma$. Also shown are predictions from various models (see text).


[5] F.M. Borzumati, B.A. Kniehl and G.Kramer: *Z. Phys.* **C59** (1993) 341;
B.A. Kniehl and G.Kramer: *Z. Phys.* **C62** (1994) 53;
B.A. Kniehl: *hep-ph/9709261 and proceedings of the Ringberg Workshop "New trends in HERA Physics", Ringberg Castle, Germany* (25-30 May 1997) ;

[6] M. Glück, E. Reya and A. Vogt: *Phys. Rev.* **D46** (1992) 1973;

[7] M. Glück, E. Reya and A. Vogt: *Z. Phys.* **C67** (1995) 433;

[8] H. Abramowicz, K. Charchula and A. Levy: *Phys. Lett.* **B269** (1991) 458;

[9] V. Blobel: *DESY 84-118 and proceedings of the CERN School of Computing, Aiguablava* (Spain) CERN 1985;

[10] G. Marchesini et al.: *Comp. Phys. Comm* **67** (1992) 465;

[11] H. Jung: *Comp. Phys. Comm.* **86** (1996) 147;

[12] M. Drees and R. Godbole: *Phys. Rev.* **D50** (1994) 3124;

[13] G.A. Schuler and T. Sjöstrand: *Phys. Lett.* **B376** (1996) 487;

[14] S.D. Ellis and D.E. Soper: *Phys. Rev.* **D48** (1993) 3160;
S. Catani et al.: *Nucl. Phys.* **B406** (1993) 187;

[15] G. D'Agostini: *Nucl. Instr. and Meth.* **A362** (1995) 487;